Uncertainties in radar echo top heights used for hail detection

Laurent Delobbe[1] & Iwan Holleman[2]

[1]*Royal Meteorological Institute of Belgium (RMI), Observations Department, Avenue Circulaire 3, B-1180 Brussels, Belgium*

[2]*Royal Netherlands Meteorological Institute (KNMI), P.O. Box 201, NL-3730 AE De Bilt, The Netherlands*

Email: laurent.delobbe@oma.be

Most operational hail detection algorithms for single-polarisation radars are based on the analysis of the vertical profiles of radar reflectivity. At KNMI (Royal Netherlands Meteorological Institute) and RMI (Royal Meteorological Institute of Belgium) the probability of hail is derived from the height of the freezing level and the 45-dBZ radar echo top height (maximum height of the 45-dBZ echo). Echo tops are affected by errors in the measured reflectivity itself and by errors in the height assigned to these reflectivities. This study investigates the quality of radar echo top heights as a function of range and explores the implications for hail detection.

The method is based on the comparison between reflectivity measurements from two radars on the vertical cross-section extending between these radars. In a first step, sampling errors related to the radar Volume Coverage Patterns are analysed using idealised storm profiles. Subsequently, real reflectivity data for 25 thunderstorm episodes are compared. It is found that the quality of the maximum reflectivity measurements strongly deteriorates with range and that about half of this degradation can be attributed to overshooting effects. Height assignment differences between the two radars are limited to about 0.5 km. Errors on the reflectivity measurements strongly affect the frequency of 45-dBZ threshold exceedances. However, once the threshold is exceeded, errors in measuring the 45-dBZ echo top heights generally affect the derived probability of hail by less than 20%.

1. Introduction

In current operational networks most radars are single wavelength and single polarisation. Various methods have been proposed for detecting hail using reflectivity measurements from this type of radar. Most hail detection methods based on single polarisation measurements rely on the analysis of the vertical profile of reflectivity.

The most straightforward method is based on Plan-Position Indicator (PPI) or Constant Altitude PPI (CAPPI) products at low levels. Mason (1971) proposed a reflectivity threshold of 55 dBZ for distinguishing between rain and hail. Auer (1972) suggested thresholds of 50 dBZ and 60 dBZ for hail of diameters larger than 8 mm and 35 mm, respectively. This method is successful in cases of severe hailstorms but does not allow one to distinguish between heavy rain and relatively small hail. The vertically integrated liquid water (VIL) is another indicator of the severity of a storm cell,

which was introduced by Greene & Clark (1972). However, discriminating between thunderstorms with and without hail using VIL only is not straightforward because there is a large variability in the VIL threshold associated with the presence of hail. Lenning et al. (1998) found that VIL was promising for indicating the presence of hail if the appropriate threshold could be determined in advance. VIL Density, i.e. the VIL normalised by the echo top height, has been proposed by Amburn & Wolf (1997). The determined threshold for the VIL Density is appropriate under widely varying VIL values, echo tops and air mass characteristics (Amburn & Wolf 1997). For strongly tilted storms, the vertical integration of liquid water may be a poor indicator of the storm severity. In Stumpf et al. (2004), a cell-based VIL is calculated using the Storm Cell Identification Algorithm (SCIT; Johnson et al. 1998). For each elevation scan, the maximum reflectivity within the storm is used to derive the VIL. In this way, the VIL is maximised by taking the reflectivity values along a tilted or even twisted reflectivity core.

The measured reflectivity depends on the number of hydrometeors, their phase and their size distribution. A large number of small hailstones may reflect more energy than a small number of large hailstones. Moreover, wet hailstones reflect more than dry hailstones. The radar measures a mean reflectivity over a sample volume, which may be filled by a mixture of hailstones and liquid particles. This implies that there is no direct relationship between the measured reflectivity and the density and size of hailstones. As a result, hail detection methods based only on radar reflectivity measurements show limited ability in diagnosing hail. For this reason, several hail detection algorithms have been proposed that make use of radar measurements in conjunction with other meteorological information such as temperature profiles.

An enhanced hail detection algorithm has been developed at the National Severe Storms Laboratory (NSSL) (Kessinger et al. 1995; Witt et al. 1998). The detection of hail of any size is based on the criterion proposed by Waldvogel et al. (1979). The probability of hail is derived from the difference between the maximum height at which a reflectivity of 45 dBZ is observed (45-dBZ echo top) and the height of the freezing level. Hail cells were only observed when the height difference was at least 1.4 km (Waldvogel et al. 1979). The probability of hail increases with the height difference. A severe hail algorithm (diameter > 19 mm) is also described in Witt et al. (1998). It is based on a severe hail index (SHI) derived from the vertical profiles of reflectivity and temperature. The vertical profile of reflectivity is first converted to a vertical profile of hail kinetic energy flux and then vertically integrated using a temperature-based weighting function. The maximum expected hail size is also derived from the SHI using a simple empirical relationship. Another hail detection method was developed and tested in the framework of the Sydney 2000 Forecast Demonstration project (Joe et al. 2004; Treloar 1998). It is an empirically-based algorithm in which the freezing level, VIL and the 50-dBZ echo top are used to predict hail size.

Auer (1994) and Hardaker & Auer (1994) proposed a method to diagnose hail which combines radar reflectivity data with infrared cloud-top temperatures from satellite imagery. This method has been extensively tested on hail cases in New Zealand and is seen to perform much better than the CAPPI method. The cloud-top temperature provides additional information on the vertical extent of the thunderstorm cells. At NSSL, an improved hail diagnosis algorithm was developed which uses a neural network that integrates reflectivity radar information with velocity radar information as well as near-storm environment variables from mesoscale models (Marzban & Witt 2001). Recent developments at NSSL concern the improvement of single-radar warning decision systems by integrating information from multiple radars, mesoscale models, satellite and lightning detection systems (Stumpf et al. 2003, 2004).

The hail detection method based on Waldvogel et al. (1979) was operationally implemented at KNMI (Royal Netherlands Meteorological Institute) in 2001 and tested on an extended verification dataset in the summer months of 1999 and 2000 (Holleman et al. 2000; Holleman 2001). The results show that, for this dataset, the Waldvogel method performs substantially better than any other tested method. The verification results have been used to adjust the function that relates the probability of hail (POH expressed in fraction) to the height difference (ΔH) between the 45-dBZ echo top and the freezing level estimated from an operational numerical weather prediction model. The following expression was obtained:

$$POH = 0.319 + 0.133\,\Delta H\,(km) \qquad (1)$$

From this equation it appears that a positive probability of hail, i.e. a POH > 0, is obtained when the maximum reflectivity exceeds 45 dBZ and the height difference ΔH exceeds −2.4 km. The same algorithm was implemented at the Royal Meteorological Institute of Belgium (RMI) in 2003. A validation study was performed in the summers of 2002, 2003 and 2004. In 83 reported hail cases, 78 were detected with a probability of hail higher than 50% at less than 10 km from the reported hail location (Delobbe et al. 2005). Unfortunately, this study did not allow the estimation of the False Alarm Rate. It is worth noting that hailstorms with reflectivity factors less than 45 dBZ have already been reported, for example in Spain (Fraile et al. 2001). Such hailstorms are not detected with the Waldvogel algorithm.

A common feature of most hail detection methods is that they require reliable measurements of the vertical profile of reflectivity. Radar reflectivity measurements are affected by various sources of error. Calibration errors, side lobe effects, shielding, attenuation and overshooting of precipitation echoes below the scanned volume are the most important ones. Some of these errors tend to increase with distance from the radar. Another important range effect is related to the increasing size of the sample volume with range. Radar measurements are not point observations. All scatterers within a given sample volume contribute to the measured reflectivity (e.g. Doviak & Zrnic 1993; Collier 1996). For a 1° beam width and a 500-m resolution in range, the reflectivity at 100-km range represents an average over an approximate volume of 1.2 km³. This averaging effect may strongly affect the measured maximum reflectivity along the vertical. Attenuation is caused by absorption and scattering by atmospheric gases, cloud droplets and precipitation. The latter contribution is by far the most substantial. Scarchilli et al. (1993) have shown that specific attenuation by intense precipitation can be as high as 0.5 dBkm^{-1} at C-band frequencies. The absolute attenuation through large thunderstorm cells can easily be several decibels. When the storm is close to the radar, a considerable shielding effect may occur over a large azimuthal sector.

Table 1. *Relevant parameters of the De Bilt and Wideumont 15-minute volume scans.*

	De Bilt	Wideumont
Location	52°6′N, 5°11′E	49°54′N, 5°30′E
Antenna height	50 m a.s.l.	585 m a.s.l.
Rotation speed	24 deg.s^{-1}	24 deg.s^{-1}
PRF	400 Hz	483 Hz
Pulse width	2 µs	2 µs
Radial resolution	1 km	500 m
Azimuthal resolution	1 deg.	1 deg.
Number of samples	65	40
Number of elevations	14	10
Elevation angles (deg.)	0.3, 0.8, 1.3, 1.8, 2.3, 2.8, 3.3, 4.0, 5.0, 6.0, 7.5, 9.0, 10.5, 12.	0.5, 1.2, 1.9, 2.6, 3.3, 4.0, 4.9, 6.5, 9.4, 17.5

Attenuation is also caused by the radome, especially when it is wet. This contribution is not, however, range dependent. The effect of attenuation on hail detection has not been addressed specifically in this study.

Vertical profiles of reflectivity are also affected by the accuracy of the height assignment of the precipitation echoes. This accuracy is limited by the antenna beam width and by the limited number of elevation angles (Howard et al. 1997; Maddox et al. 1999). Furthermore, errors on the height assigned to the measured reflectivities arise due to the uncertainties in the trajectories of the radar beams. These uncertainties are related to inaccurate antenna pointing and to variations of the atmospheric propagation conditions resulting from variations in the vertical refractivity gradient (e.g. Bech et al. 2003).

The aim of this study is to investigate the quality of radar echo top heights as a function of range and to discuss the implications for hail detection. The methodology is based on the comparison between reflectivity measurements from the radar at De Bilt in The Netherlands and the radar at Wideumont in Belgium. Both radars are Gematronik C-band Doppler radars. They perform a volume scan every 15 minutes. Some relevant parameters of these scans are given in Table 1. The distance between the two radars is 244 km. The intersection line is entirely over land. The beam geometry of the two radars is shown in Figure 1 using the format of Maddox et al. (1999).

As a first step, a theoretical study based on idealised storm profiles is presented. In this study, the apparent reflectivity profiles seen by the two radars are determined as a function of range for three different idealised profiles in order to estimate the apparent maximum reflectivity along the vertical and the echo top heights. The goal is to identify the sampling errors related to the Volume Coverage Patterns (VCPs) of the two radars. The second step involves comparing real storm reflectivity data from the two radars. Usually, comparisons of reflectivity data measured by two or more radars are based on PPI or CAPPI products (e.g. Huuskonen 2001; Tabary 2003), but this does not allow one to identify errors related to height assignment as a function of range. Here, the comparison of reflectivity data is made on a vertical cross-section extending from one radar to the other. The reflectivity field observed at a short distance by one radar is considered to be representative of the storm structure. By comparing the reflectivity fields observed at the same time and location by two widely separated radars it is possible to identify the shortcomings associated with observing storms that are far removed from the radar site.

2. Theoretical study using idealised storm profiles

An important source of error stems from the sampling limitation of radar measurements related to the Volume Coverage Pattern (VCP). The vertical profile of reflectivity is derived from a limited number of elevation scans and, for each elevation scan, the reflectivity is averaged over a given beam volume determined by the antenna beam pattern. In this section, the results are described of a theoretical study of the potential impact
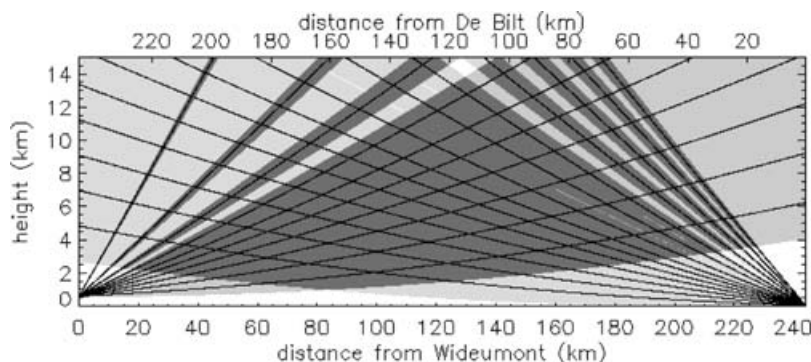

Figure 1. *Radar beam geometry for the radars at Wideumont (located on the left) and De Bilt (located on the right). Regions sampled by both radars are in dark grey; regions sampled by one radar are in light grey; regions in white are not sampled. Solid lines indicate the centres of the radar beams.*
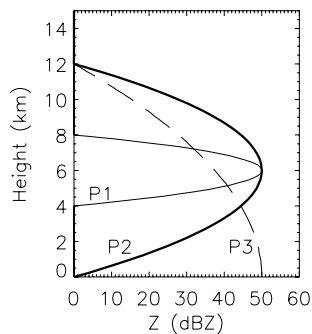
Figure 2. *Vertical reflectivity profiles for the three idealised storms P1, P2 and P3.*

Figure 3. *(a) Apparent Z_{max} and (b) apparent 30- and 45-dBZ ETPs seen by the radar at Wideumont (solid line) and the radar at De Bilt (dashed line) for idealised profile P1. Thin and thick lines in (b) correspond to 30 and 45 dBZ, respectively. The dotted lines indicate the real ETPs.*

of sampling errors on the differences in maximum reflectivity and echo tops measured by the two radars. This study is based on a simulation of the apparent vertical reflectivity profiles measured by the two radars as a function of range for a number of idealised storm profiles. The storm is assumed to be located on the line between the two radars. In Howard et al. (1997), radar measurement uncertainties are analysed using a vertical reflectivity structure model for the life cycle of an idealised 'single-pulse' thunderstorm. In the present study, three different parabolic profiles (P1, P2 and P3), corresponding to the pulse-type storm at three different stages of its life cycle, have been considered. Figure 2 shows the three profiles P1, P2 and P3 corresponding to the growth, maturity and decay stages, respectively. All profiles have a maximum reflectivity of 50 dBZ. For each idealised profile, the apparent profile seen by the two radars is calculated as a function of range assuming a Gaussian power distribution within the 3-dB beam width. The apparent maximum reflectivity and echo tops for different reflectivity thresholds are derived from the apparent profiles. Echo tops are determined using linear vertical interpolation of the reflectivity from the beam centre values.

Figure 3a shows the apparent maximum reflectivity (Z_{max}) as a function of range for the two radars and for profile P1. At very short ranges from the radars, the maximum reflectivity core is located at an altitude not scanned by the radar (the so-called cone-of-silence), which results in a strong underestimation of Z_{max}. Up to about 50 km, very large variations of the apparent Z_{max} are obtained for the Wideumont radar due to the large vertical gaps between the high elevation scans (undersampling effect). The larger number of high elevation scans used by the De Bilt radar strongly reduces this effect. At long ranges, both radars detect an apparent Z_{max} around 45 dBZ. Inspection of Figures 1 and 2 shows that no overshooting occurs. The 5-dBZ underestimation is entirely attributable to the averaging within the radar beam volume.

The apparent echo tops for 30-dBZ and 45-dBZ thresholds have been calculated and the results are shown in Figure 3b. The apparent echo top (ETP) does
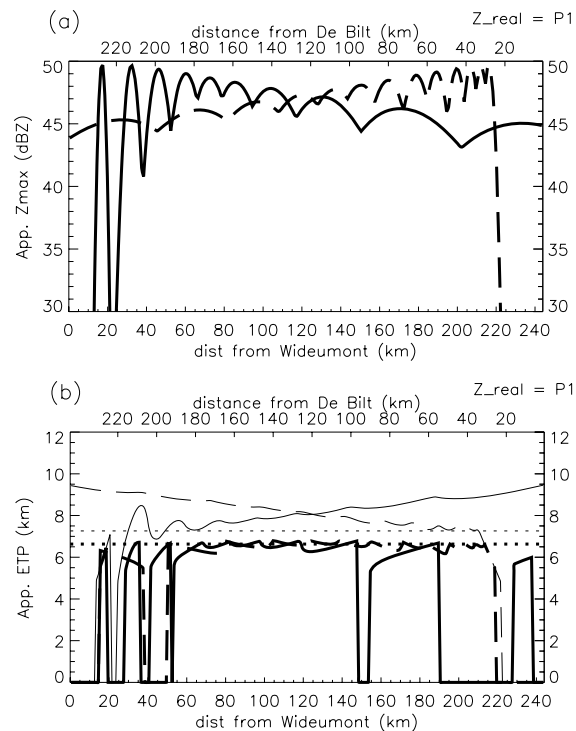
not exist at ranges where the apparent Z_{max} drops under the threshold. The actual 30-dBZ and 45-dBZ ETPs are 7.26 and 6.63 km, respectively. Except at short range, the sampling errors result in an overestimation of the 30-dBZ ETP. This overestimation increases with range as a result of the increasing beam volume. The apparent 30-dBZ ETP at 200 km from the radar is around 9 km for both radars, which means an overestimation by about 1.75 km. At ranges where it exists, the apparent 45-dBZ ETP is in good agreement with the real ETP. Errors are limited to about 0.5 km. However, the 45-dBZ threshold is not exceeded in large range intervals. At short range, it is due to the undersampling resulting from the vertical gap between the elevation scans. At long range, it is due to the averaging effect. The core of reflectivity higher than 45 dBZ has a vertical extension of 1.26 km and only partially fills the radar beam volume.

The results obtained with the idealised profiles P2 and P3 are shown in Figures 4 and 5. For profile P2, the range dependence of the apparent Z_{max} and ETPs is reduced with respect to profile P1. At long range, the underestimation of Z_{max} is limited to about 2 dBZ. The averaging effect is less pronounced since profile P2 is smoother than P1. The 30- and 45-dBZ ETPs are relatively well estimated by both radars except at short ranges. The overestimation at long range is more pronounced for the 30-dBZ ETP but remains limited to 1 km at 200 km range.
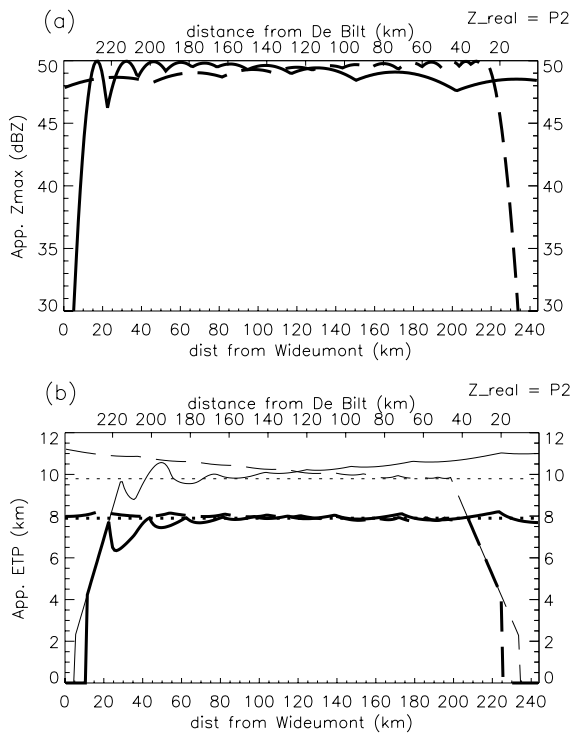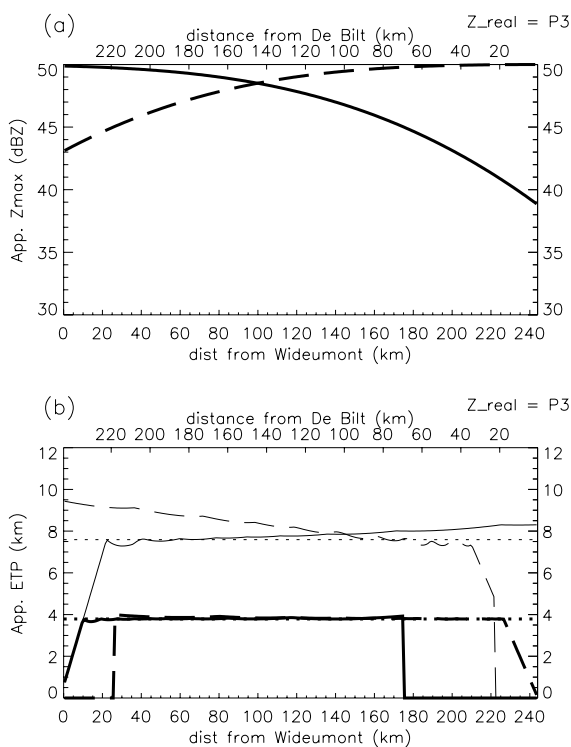
Figure 4. *As for Figure 3 but for profile P2.*

Figure 5. *As for Figure 3 but for profile P3.*

For profile P3, the high reflectivity core is located near the ground, which implies that overshooting has a significant impact. A strong decrease of the apparent Z_{max} with range can be seen in Figure 5. This effect is more pronounced for the radar at Wideumont. This is related to the VCPs of the two radars. The lowest scanned elevation is $0.5°$ for Wideumont while it is

$0.3°$ for De Bilt. As a consequence, overshooting effects are likely to occur at shorter ranges for the radar at Wideumont. The orography amplifies this effect since the radar at Wideumont is located near the top of the Ardennes ridge at 585 m ASL, while the radar at De Bilt is located at 50 m ASL. At long ranges, the apparent Z_{max} drops under the 45-dBZ threshold, which results in the non-existence of the 45-dBZ ETP. Where it exists, the 45-dBZ ETP is correctly estimated by both radars.

The difference between the Z_{max} and ETPs seen by the radars at Wideumont and De Bilt for the three idealised profiles is shown in Figure 6. For profile P2, differences in Z_{max} are between -2 and $+2$ dB except at very short ranges. Larger differences are obtained with profiles P1 and P3. For profile P1, the effect of undersampling is large due to the large vertical gradients of the reflectivity profile. For profile P3, the overshooting effect is the dominant source of discrepancies between the two radars. In the range interval 40–200 km, the Zmax differences are between -5 and $+5$ dB for both profiles. Differences in 30- and 45-dBZ ETPs are shown in Figures 6b and 6c. Large differences are obtained at short ranges from the radars due to the presence of the cone-of-silence and the undersampling at high elevation by the radar at Wideumont. For ranges between 40 and 200 km, differences in 30-dBZ ETP are typically between -1.5 and $+1.5$ km. Smaller differences are obtained for the 45-dBZ threshold at ranges where this threshold is exceeded in both radar apparent profiles.

The results of the theoretical study presented here are, of course, influenced by the choice of the idealised profiles. Nevertheless, it facilitates a better understanding of the combined effect of the Volume Coverage Pattern and the shape of the vertical profile of reflectivity on the apparent Z_{max} and ETPs. Sampling errors always result in an underestimation of Z_{max}. The apparent Z_{max} depends on the shape of the VPR within the beam volume. Large vertical gradients will cause a stronger underestimation. The effect of sampling errors on the ETPs is more complex. The apparent ETPs can be either underestimated or overestimated and the difference between the actual and the apparent ETPs depends on the apparent Z_{max} at the different elevations but also on the shape of the VPR between the beam centres and on the interpolation scheme used to extract the ETP. A significant overestimation of the ETP may occur at long range when the lower part of the radar beam intercepts a reflectivity core that is substantially larger than the ETP threshold. In this case, the apparent reflectivity will be larger than the real reflectivity at the altitude of the beam centre.

The Z_{max} and ETP errors identified in this theoretical study are exclusively caused by radar sampling effects. Even if the three idealised profiles tested here cannot be considered to be representative of all storm situations, it gives a first idea of the magnitude of the errors which can be expected without the additional contribution
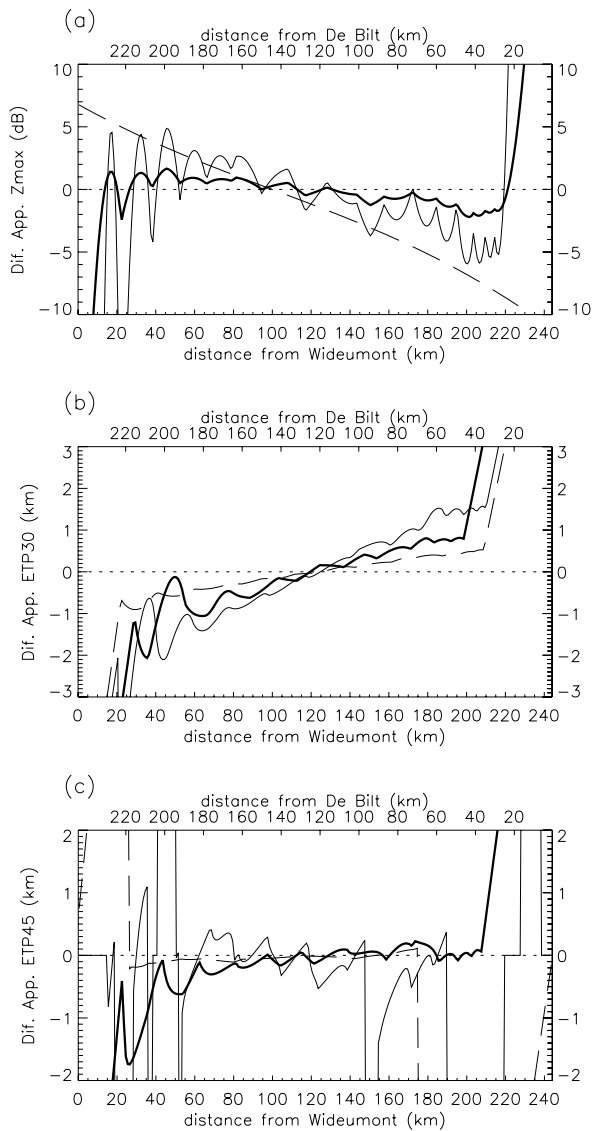
365

Figure 6. *Differences in (a) apparent Z_{max}, (b) 30-dBZ ETP, and (c) 45-dBZ ETP between the radars at Wideumont and De Bilt for the idealised profiles P1 (thin solid line), P2 (thick solid line), and P3 (dashed line).*

Table 2. *Selected hail episodes, number of vcut pairs and mean Z_{max} difference ($Z_{max}(Wid)$–Z_{max} (DeB) (dBZ)) for each episode.*

Date	N. vcuts	Diff. Z_{max}	Date	N. vcuts	Z_{max}
20020730	20	4.64	20040708	16	1.86
20020803	9	2.73	20040709	32	4.61
20030608	12	1.72	20040717	32	3.83
20040530	40	1.07	20040718	24	−0.05
20040531	28	−0.42	20040721	36	0.87
20040602	60	1.15	20040722	8	−2.03
20040610	63	3.09	20040723	16	0.92
20040612	52	4.28	20040824	48	2.46
20040619	28	0.53	20040825	48	3.94
20060620	48	3.15	20040830	32	−0.27
20040623	32	3.92	20040910	32	2.32
20040702	16	4.14	20040911	96	2.66
20040707	44	2.81			

of calibration errors, attenuation or variations in beam propagation. This analysis will serve as a baseline for the comparison using real storm data.

3. Comparison using measured reflectivity data

3.1. Method

For each radar, the reflectivity field on a vertical cross-section (denoted hereafter: 'vcut') in the direction of the other radar can be extracted from the volume data. First comparisons of vertical cross-sections based on a small number of thunderstorm cases have been presented by Delobbe & Holleman (2003, 2004). In the present study, 25 thunderstorm days in the summers of 2002, 2003 and 2004 are considered. Cases with significant anomalous propagation giving rise to significant ground echoes were eliminated through a visual inspection of the vcut

pairs. None of the vcut pairs shows three-body scatter (Lemon 1998). The number of selected vcut pairs for each storm episode is given in Table 2. A total of 872 vcut pairs have been selected. The time difference between the corresponding volume datasets never exceeds 3 minutes. Nevertheless, the storm evolution within this time interval will contribute to differences between the two radar datasets. The sample has been further reduced by rejecting the vcuts where the maximum reflectivity (Z_{max}) is less than 7 dBZ in both datasets, which is the lowest reflectivity level on the radar displays of RMI and KNMI. The number of vcut pairs where Z_{max} exceeds 7 dBZ in at least one of the two vcuts is 845. Among these vcut pairs, the number of pairs where Z_{max} exceeds 20 dBZ, 30 dBZ, and 45 dBZ is 764, 609, and 181 respectively.

Figure 7 shows an example of a vcut pair. Three distinct cells are seen between the two radars. The vertical extensions and the reflectivity levels are quite similar in both datasets. One of the three cells exhibits reflectivity values higher than 45 dBZ. Some differences in the vertical structure of that cell can be observed but in the present case the difference in the 45-dBZ echo top does not exceed 1 km. According to (1), the impact on the probability of hail for this case is limited to 13%.

In many cross-sections, ground clutter caused by side-lobe effects is present up to a distance of about 40 km. Further, measurements at short range are strongly affected by the cone-of-silence. For this reason, the comparison of reflectivity data has been limited to ranges between 44 and 200 km. This range domain, which is symmetric around the middle point between the two radars, has been divided into 15 range intervals. All intervals are 10-km wide except the two extreme ones which are 13-km wide. For each interval, four different variables have been compared: (a) maximum reflectivity along the vertical within the range interval
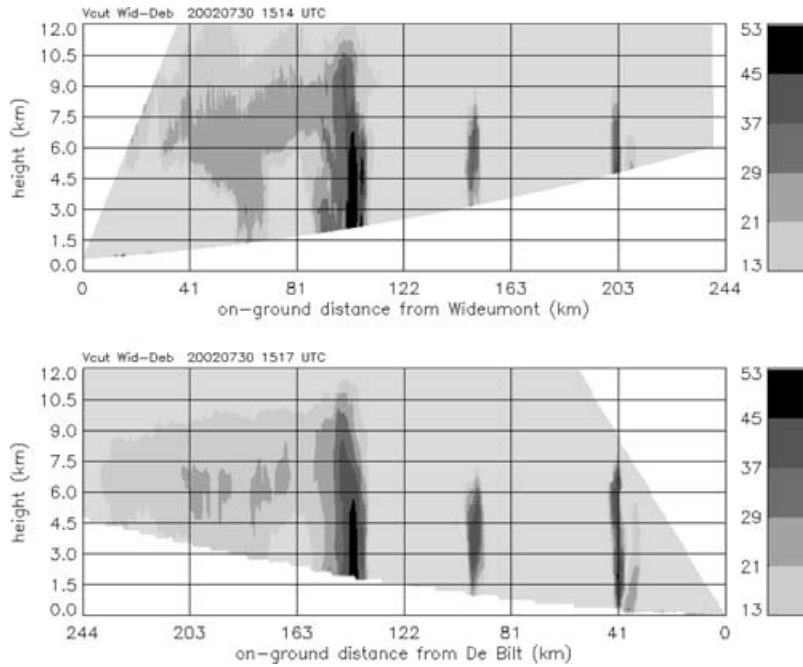
Figure 7. *Reflectivity (dBZ) on a vertical cross-section Wideumont–De Bilt observed by the Wideumont radar (upper panel) and by the De Bilt radar (lower panel). The distance between the two radars is 244 km.*

(Z_{max}), (b) height of the measured maximum reflectivity (H_{Zmax}), (c) echo top for different thresholds (ETP) and (d) threshold exceedance.

The comparisons have been carried out following two different methods. In the standard method, the variables within a given range bin are compared even if the Z_{max} measured by one radar is observed at an altitude which falls outside the volume scanned by the other radar. It means that a Z_{max} observed at low altitude at short range from one radar will be compared to a Z_{max} observed at a higher altitude by the other radar. Using this method of comparison, overshooting effects will contribute to the differences between the two radars. In the second method, a range bin will be included in the comparison only if the Z_{max} measured by one radar is observed at an altitude covered by the other radar. This second method allows for the elimination of the contribution of overshooting to the discrepancies between the two radar datasets. The two methods are hereafter denoted 'standard' and 'no_overshoot'.

3.2. Z_{max} difference

Maximum reflectivity along the vertical is not affected by the heights assigned to the reflectivity measurements at the different beam elevations. Therefore, the comparison of maximum reflectivity values measured by the two radars permits the elimination of the effect of height assignment errors resulting from inaccurate antenna pointing and variations in atmospheric propagation. Figure 8 shows the effect of range on the mean difference between the maximum reflectivity of the two radars obtained using the standard method of comparison. The comparison has been performed for three different

thresholds: 7 dBZ, 20 dBZ and 30 dBZ. For each range interval, only vcut pairs with maximum reflectivity values higher than the threshold in both datasets are considered. With a low threshold of 7 dBZ, comparisons are based on a large number of vcut pairs, which makes it possible to identify calibration differences between the two radars. The results obtained with 20- and 30-dBZ thresholds are not shown here. These results are very close to those obtained with a 7-dBZ threshold. The comparison of the mean Z_{max} difference was not made for a 45-dBZ threshold because the number of valid pairs per range interval is too small. The number of valid pairs per range interval and the standard deviation of the Z_{max} difference are also shown on Figure 8. The number of valid pairs is around 300 and the standard deviation is between 6 and 10 dBZ for all ranges.
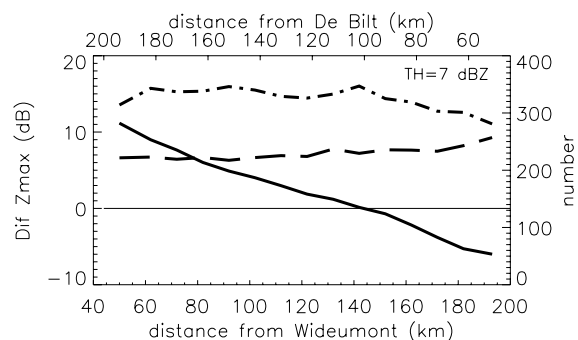

Figure 8. *Mean Z_{max} difference Wideumont–De Bilt (solid line), standard deviation of the Z_{max} difference (dashed line) and number of valid pairs per 10-km range interval (dash-dotted line) as a function of range using the standard method for a reflectivity threshold of 7 dBZ. Only vcut pairs with maximum reflectivity higher than the threshold in both datasets are considered as valid.*
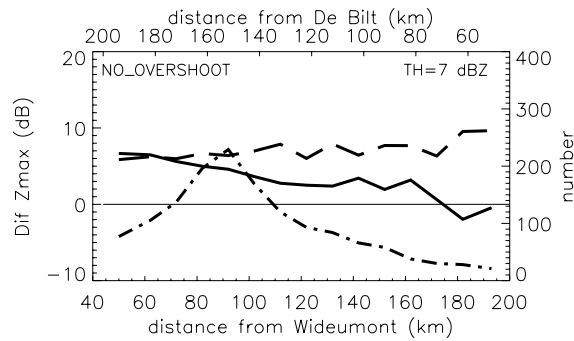
367

Figure 9. *As for Figure 8 but with the no_overshoot method of comparison.*

The results obtained using the no_overshoot method of comparison are presented in Figure 9. When this method of comparison is used, the number of valid pairs is smaller and strongly depends on range. A peak number of vcuts is obtained at 90 km from the radar at Wideumont. At this range, the lowest beams of the two radars are at the same altitude and the vertical portion of the troposphere covered by the two radars is the same, as can be seen on Figure 1. At short range from De Bilt, the number of valid pairs is extremely low. This means that a large number of maximum reflectivity cores detected by the radar at De Bilt are missed by the radar at Wideumont. This is related to the VCPs of the two radars, which implies that overshooting effects are likely to occur at shorter ranges for the radar at Wideumont than for the radar at De Bilt.

The mean difference of Z_{max} using the standard method shows a linear variation with range. At short ranges from Wideumont, the Z_{max} measured by the Wideumont radar exceeds the Z_{max} measured by the radar at De Bilt, with a mean difference of 11 dB at 50 km. At long ranges, the opposite behaviour is observed with reflectivities from De Bilt exceeding those from Wideumont by about 6 dB at 194 km from Wideumont (50 km from De Bilt). Averaged over all ranges, the mean Z_{max} measured by the Wideumont radar displays a bias of +2.1 dB.

Comparison of Figures 8 and 9 shows that the results obtained with the two methods are different. When the effect of overshooting is eliminated from the comparison, the range dependence of the Z_{max} differences is reduced. Specifically, the mean slope is reduced by a factor of two, which suggests that about half of the range dependence of Z_{max} can be attributed to overshooting at increasing ranges. It implies that other sources of error, like the attenuation and the increasing size of the sample volume, also contribute to the range effect. Averaged over all ranges, the mean difference in Z_{max} is +3.0 dB for the no_overshoot method. This mean bias, which is not affected by overshooting, and, which is based on a large number of comparisons (1451 Z_{max} pairs), can be considered as the mean calibration bias between the two radars. Nevertheless, it should be kept in mind that calibration differences between the two radars may vary in time. The 3.0-dB bias is an

average over all selected thunderstorm episodes. The calibration bias has been estimated for each episode using the same method based on the comparisons of Z_{max} (see the results in Table 2). For each episode, the estimated bias is based on a relatively small number of vcut pairs and may be affected by errors not related to calibration. Therefore, the mean Z_{max} difference is probably a poor estimate of the calibration bias for a given storm episode. A better evaluation of calibration differences between the radars could be obtained by comparing all data sampled by the radars at the same three-dimensional location (Gourley et al. 2003). This analysis, which should not be restricted to convective storm cases, is beyond the scope of the present study.

The method of comparison hardly affects the standard deviation of the Z_{max} differences. Looking at Figure 6a showing the results of the theoretical study, it appears that the standard deviation is relatively large compared to the differences which can be expected from sampling errors only, especially at intermediate ranges. This suggests that sampling errors are only partially responsible for the differences in the reflectivity values measured by the two radars. Calibration differences and attenuation also play an important role.

3.3. Z_{max} height difference

Echo top heights are sensitive to reflectivity values measured by the radar but also to the heights assigned to the measured reflectivities H_{Zmax}. In order to identify height assignment errors, the height where the maximum reflectivity is observed has been extracted for each range bin from both radars and the mean value for each of the 15 range intervals has been determined. Note that H_{Zmax} differences are not affected by calibration differences between the two radars since these differences do not affect the shape of the vertical profile of reflectivity.

Differences in the heights assigned to maximum reflectivity are caused by errors in the antenna pointing, by variations in the atmospheric propagation conditions, and by the sampling errors resulting from the beam size and the limited number of elevation angles. Another effect is related to differential attenuation, i.e. the attenuation is not the same for the different elevation angles which may introduce a vertical shift of the position of the maximum reflectivity for a given precipitation cell.

As for Z_{max} the comparisons were made for three different thresholds: 7 dBZ, 20 dBZ and 30 dBZ. With a higher threshold, only the altitudes of high reflectivity cores are compared. Figure 10 shows the differences between H_{Zmax} observed from Wideumont and De Bilt radars using the two methods of comparison for the 7-dBZ threshold. The difference in Z_{max} heights obtained using the standard method shows a linear dependence with range. At 50 km from Wideumont, the mean height difference is −1 km. At 190 km from Wideumont
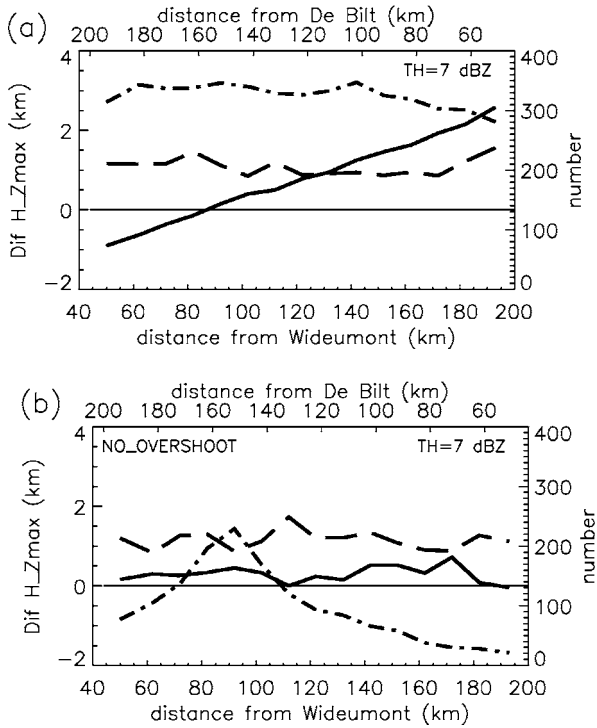
Figure 10. *Mean Z_{max} height difference Wideumont–De Bilt (solid line), standard deviation of the Z_{max} height difference (dashed line) and number of valid pairs per 10-km range interval (dash-dotted line) as a function of range for a reflectivity threshold of 7 dBZ (a) with the standard method of comparison, and (b) with the no_overshoot method.*

(50 km from De Bilt), the height difference reaches 2.5 km. At this range, the difference in altitude of the lowest beams of the two radars reaches 4 km. In many cases, the radar at Wideumont overshoots the maximum low-level reflectivity core observed by the radar at De Bilt. Around 90 km from Wideumont, the mean height difference is close to zero. As mentioned above, the two radars scan the same vertical portion of the atmosphere around this range. The results obtained with larger thresholds are similar.

When the no_overshoot method of comparison is used, the mean height differences are greatly reduced (Figure 10b). The differences are limited to about 0.5 km for all ranges except at 172 km from Wideumont where it reaches a maximum of 0.7 km. The radar at Wideumont tends to assign larger heights to the measured reflectivity values but the differences are low compared with the vertical resolution of the radar measurements. It suggests that overshooting is the main source of differences between the heights of maximum reflectivity observed by the two radars. In other words, when this effect is eliminated, systematic differences in the heights assigned to the maximum reflectivity are rather low for all ranges. This result and the absence of bias at 90 km indicate that the mean antenna pointing of both radars is accurate.

The standard deviation of the height differences is also shown in Figure 10. The results obtained using the

two methods of comparisons are similar. The range dependence is low and the mean standard deviation is around 1.3 km. This standard deviation is comparable to the beam size at intermediate range and to the vertical distance between the elevation beams, as shown in Figure 1. This suggests that differences in Z_{max} height can be entirely attributed to sampling errors. The contributions of inaccurate antenna pointing, variations in atmospheric propagation and differential attenuation appear to be limited.

The results obtained near De Bilt with the standard method of comparison show that the difference in the VCPs of the two radars substantially affects the performances at long ranges. Using a lowest elevation angle of 0.3° instead of 0.5° allows a significant increase in the effective range for which reliable measurements of the vertical structure of the reflectivity field can be obtained. The low altitude of the radar at de Bilt is also beneficial for long-range measurements.

3.4. Differences in echo tops

The echo top values have been calculated for the two radars and for three thresholds: 7 dBZ, 20 dBZ and 30 dBZ. For both radars, the echo top is estimated through a linear vertical interpolation from the beam centre reflectivity values. For each range interval, only vcut pairs where the echo top exists (i.e. where the maximum reflectivity exceeds the threshold) in both datasets are included in the calculation of the mean difference. Cases where the threshold is exceeded in one dataset and not in the other are not treated here. Differences in echo top values are caused by differences in the measured reflectivities and in the heights assigned to these reflectivities, which makes the interpretation of the echo top discrepancies more difficult.

The mean difference of ETP between Wideumont and De Bilt for 7-dBZ, 20-dBZ, and 30-dBZ thresholds are shown in Figures 11, 12 and 13. For both methods of comparison and for all thresholds the echo top differences are smaller than 1.5 km except at short range from the radar at De Bilt. Using the standard method the differences in ETP are smaller than those obtained for H_{Zmax}. This is probably due to the fact that for a given threshold the ETP is always observed at a higher altitude than the maximum reflectivity. As a consequence, the effect of overshooting is less apparent. The no_overshoot method of comparison consists here in including the vcut pairs only if the echo top is observed by each radar at an altitude covered by the other radar. The range dependence of the echo top differences is significantly reduced when the no_overshoot method is used.

Figure 13a can be compared with Figure 6b showing the 30-dBZ ETP differences for the three idealised profiles. In both figures, there is a similar increase in these
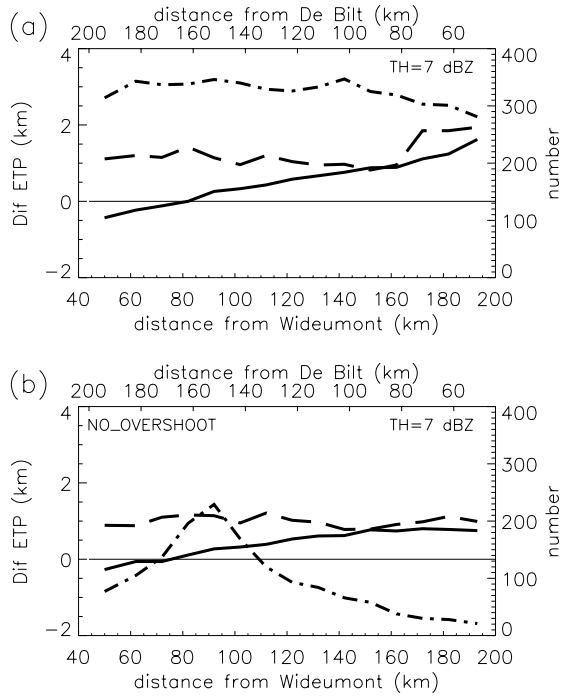
Figure 11. *Mean 7-dBZ echo top difference Wideumont–De Bilt (solid line), standard deviation of the 7-dBZ echo top difference (dashed line) and number of valid pairs per 10-km range interval (dash-dot line) as a function of range (a) with the standard method of comparison, and (b) with the no_overshoot method.*
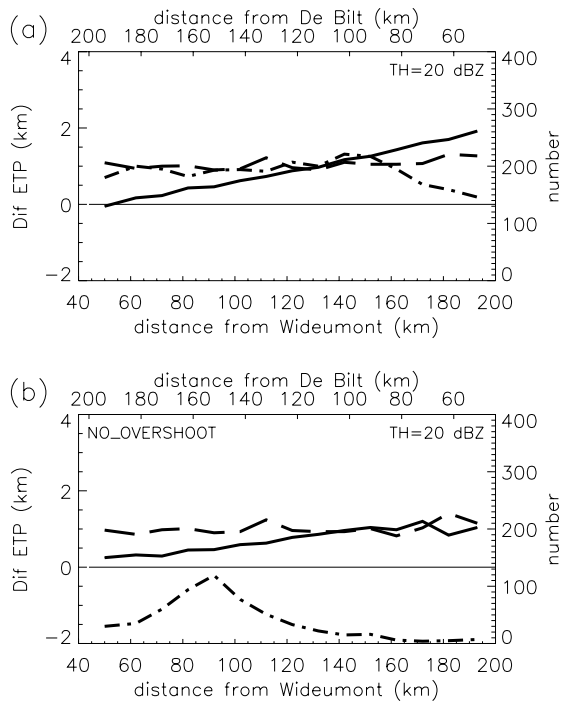

Figure 12. *As for Figure 11 for a 20-dBZ threshold.*

Figure 13. *As for Figure 11 for a 30-dBZ threshold.*

differences with the distance from Wideumont. The theoretical study has shown that these differences are related to the overestimation of the ETP at long range. Due to the calibration bias between the two radars, the ETP differences obtain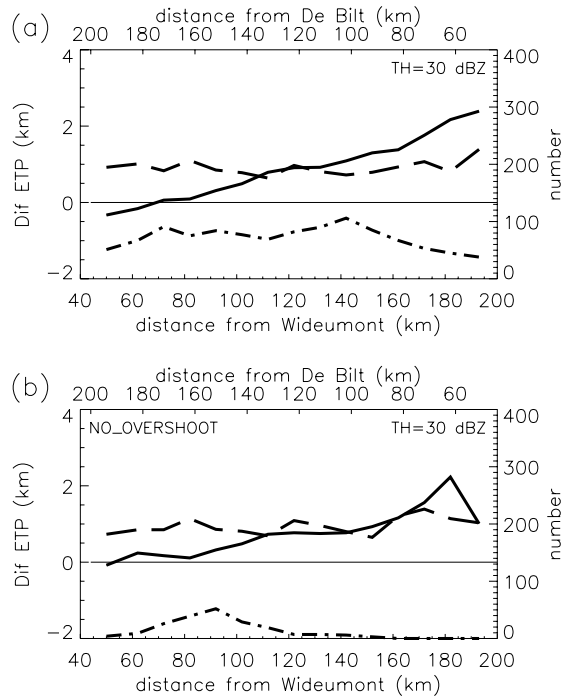ed with the real storm data are positively biased. The slope of the ETP differences as a function of range are similar in both figures, which suggests that the range dependence is mostly due to sampling errors. The standard deviation is also given in Figures 11, 12 and 13. It is close to 1 km for all ranges and all thresholds except at close range from De Bilt for the 7-dBZ threshold using the standard method of comparison. This is probably due to ETP values measured by the radar at Wideumont in the cone-of-silence of the radar at De Bilt.

As mentioned above, the number of range intervals where the 45-dBZ threshold is exceeded in both datasets is too small to produce significant results. However, the echo top differences obtained with 7-dBZ, 20-dBZ, and 30-dBZ thresholds are very similar. Whatever the threshold, the echo top differences rarely exceed 1.5 km. The same order of magnitude can be expected for a 45-dBZ threshold. Therefore, our results show that the impact of height assignment errors on the derived probability of hail using the Waldvogel algorithm is relatively minor. For a given height of the freezing level, a 1.5-km change in the estimated 45-dBZ echo top affects the derived probability of hail by 20% (Eq. 1).

It is important to stress that, around the echo top threshold, small variations in the measured reflectivity values cause the detection or non-detection of the echo top. In this case, the echo top may be present in one dataset and not in the other one. This effect, which will be discussed in the next section, is not taken into account in the echo top comparisons since only the vcut pairs where the threshold is exceeded in both datasets are included in the comparison.

3.5. Number of threshold exceedances

In order to indicate the importance of the errors related to the exceedance of the threshold in only one of the two datasets, the occurrence of threshold exceedance (the number of vcuts where the threshold is exceeded) has been calculated for both radars for all range intervals. The occurrences have been determined for 30-dBZ and 45-dBZ thresholds.

The 45-dBZ exceedance is critical for operational hail detection at KNMI and RMI since the Waldvogel algorithm gives a positive probability of hail provided that this threshold is exceeded and that the 45-dBZ echo top is higher than 2.4 km under the freezing level. In Belgium and The Netherlands, the freezing level does not exceed 5 km ASL, which means that a 45-dBZ echo top higher than 2.6 km ASL gives a positive POH. This condition is realised in most cases, which means that the number of 45-dBZ exceedances is almost equal to the number of cases where a positive POH is detected.

There are 872 vcut pairs and for each vcut 15 range intervals. The number of events is thus 13080. For a given event, the threshold can be exceeded in both radar datasets, in one of the two or in none of the two. Note that all vertical cross-sections have been selected during thunderstorm episodes. In most cases, a low threshold will be exceeded in both datasets. Differences between the number of exceedances detected by the two radars are more significant for larger thresholds. The results obtained with 30 and 45-dBZ thresholds are shown in a contingency table (Table 3). For a 30-dBZ threshold, the number of exceedances detected by one of the two radars is comparable to the number of exceedances detected by both radars. For a 45-dBZ threshold, 77% of the exceedances detected by at least one radar are only detected by one of the two radars. The number of hail exceedances only detected by the radar at Wideumont is larger than those only detected by De Bilt. This is probably due to the calibration bias between the two radars.

The range dependence of the number of threshold exceedances is illustrated in Figure 14 for a 45-dBZ threshold. For this threshold, the number of exceedances can be interpreted as the number of detected
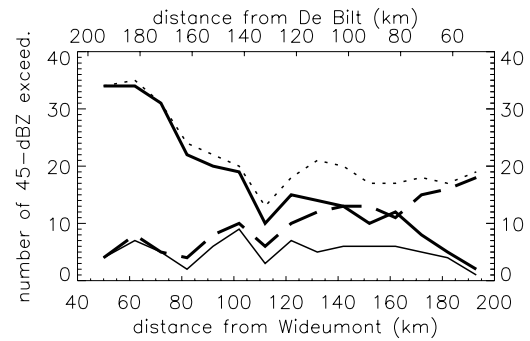

Figure 14. *Number of 45-dBZ exceedances as a function of range for the radars at Wideumont (solid line) and De Bilt (dashed line). The thin solid line shows the number of exceedances by both radars; the dotted line shows the number of exceedances by at least one radar.*

hail cases. As expected, the number of exceedances strongly varies with range. At 50 km from Wideumont, the radar at Wideumont detects 34 hail cases while the radar at De Bilt only detects four cases. At 50 km from De Bilt, the radar at De Bilt detects 18 hail cases while the radar at Wideumont detects two hail cases. For both radars, the number of detected hail cases at long range (190 km) is only 11% of the number of hail cases detected at short range by the other radar.

The best agreement between the two radars is obtained around 140 km from Wideumont (around 100 km for De Bilt). At this range the positive calibration bias of the Wideumont radar is compensated by the various range effects which tend to reduce the measured maximum reflectivity. The number of hail cases detected by both radars is shown in Figure 14 by the thin solid line. Even for intermediate ranges, hail detections by only one radar is much larger than detections by both radars. It should be noted that detection by both radars does not mean correct detection. A false alarm may be produced by both radars. The aim of the comparisons presented here is to point out the differences between the two radars and their range dependence. Verification of the hail detection product using ground observations as in, for example, Nanni et al. (2000) is not addressed in the present study.

The large differences in 30-dBZ and 45-dBZ exceedances detected by the two radars are not caused by height assignment errors. These differences are entirely attributable to errors in the measured reflectivity itself. Calibration bias, overshooting, averaging within the sample volume and attenuation are the main sources of error. These errors are clearly responsible for a significant degradation of the quality of hail detection with increasing range.

4. Summary and discussion

Uncertainties in radar echo top heights and derived hail detection have been analysed as a function of range using

Table 3. *Contingency tables giving the number of events where a given threshold is exceeded. The results are given for 30- and 45-dBZ thresholds.*

		$Z_{max} > 30\,dBZ$				$Z_{max} > 45\,dBZ$	
		Wideumont				Wideumont	
		Yes	No			Yes	No
De Bilt	Yes	1080	484	De Bilt	Yes	76	77
	No	877	10639		No	173	12754

idealised storm profiles and real storm data collected by the radar at Wideumont in Belgium and the radar at De Bilt in The Netherlands.

A theoretical study based on idealised reflectivity profiles has allowed the authors to point out sampling errors related to the Volume Coverage Patterns (VCP) of the radars. These errors result from the size of the radar beam and the limited number of elevation scans. Sampling errors cause an underestimation of the apparent maximum reflectivity along the vertical especially at short range due to the cone-of-silence and at long range due to the overshooting effect and the increasing size of the sample volume. Sampling errors cause the apparent echo tops to be either underestimated or overestimated. A significant overestimation may occur at long range when large vertical gradients are present in the vertical profile of reflectivity.

Measured reflectivity data have been compared for 25 thunderstorm episodes observed during the summers of 2002, 2003 and 2004. Vertical cross-sections extending between the two radars have been extracted from the volume data files. A total of 845 cross-sections have been extracted from both radar datasets. The first comparisons concerned the maximum reflectivity along the vertical measured by the two radars. These comparisons are a valuable tool for analysing the different sources of error as a function of range. The quantitative analysis shows that the quality of the maximum reflectivity measurements deteriorate rapidly with range and that about half of this degradation can be attributed to overshooting effects. Sampling errors resulting from the increasing size of the sample volume also play an important role, as well as attenuation and calibration errors. The comparisons made it possible to identify a mean calibration bias of 3 dB between the two radars.

All types of errors have an impact on Z_{max} measurements and their relative contributions depend on the combined effect of the radar VCP and the storm vertical profile of reflectivity. For example, sampling errors are small for a storm with a large vertical extent and a relatively uniform VPR. The precipitation pattern over the radar coverage also plays an important role. Attenuation effects will be less pronounced for an isolated thunderstorm cell than for a larger scale thunderstorm complex.

Echo top products are not only affected by errors on the measured reflectivity itself but also by errors in the height assigned to the measurements. In this study, the heights assigned to the measured maximum reflectivity were compared and it was established that overshooting is the main cause of discrepancy between the height of the maximum reflectivity measured by the two radars. When the effect of overshooting is eliminated in the comparison, the mean difference between the maximum reflectivity heights observed by

the two radars is around 0.5 km for all ranges. The standard deviation is about 1 km at all ranges. These relatively small differences can be entirely attributed to sampling errors. The contribution of inaccurate antenna pointing and variations in atmospheric propagation is very limited, given that obvious anomalous propagation cases were removed previously.

As far as echo tops are concerned, the results show that, when the reflectivity threshold is exceeded in both datasets, the differences are generally smaller than 1.5 km. The impact of such errors on the derived probability of hail using the Waldvogel algorithm as operated at KNMI and RMI is smaller than 20%. However, our results show that in many cases the 45-dBZ threshold is exceeded in one dataset and not in the other one. The exceedance of the 45-dBZ is necessary and in most cases sufficient to produce a positive probability of hail. Consequently, the hail detection algorithm is extremely sensitive to small variations in the measured reflectivity around the 45-dBZ threshold and this leads to a strong degradation of the performances of the hail detection algorithm with range. At 190 km, the number of hail cases detected by one radar is 11% of the number of cases detected by the other radar at close range. All hail diagnosis methods based on echo top products are subject to this limitation. Based on Figure 14, it is recommended that the range for hail detection using single-radar data should be limited to 150–160 km. In summary, errors on the reflectivity measurements strongly affect the number of 45-dBZ threshold exceedances; however, once the threshold is exceeded, the errors on the echo top height have a moderate impact on the derived probability of hail.

Limitations at long range of the hail detection product highlight the need to combine multiple-radar reflectivity data to estimate maximum reflectivity, echo tops and derived probability of hail. A combined hail detection product could be generated from the radars at Wideumont and De Bilt by taking, for example, the maximum of the two estimated POH. Using this method, the number of detected cases would be that given by the dotted line in Figure 14. At a range of 140 km from each radar, the number of hail detections using this dual-radar method would be twice as large as the number of detections based on single-radar measurements.

Another possible approach consists in combining three-dimensional reflectivity data from multiple radars. Nowadays, fast internet transfers and efficient compression techniques allow real time transmission of volume reflectivity files. The use of multiple-radar data to construct 'virtual volume' scans is described in Lynn & Lakshmanan (2002) and Stumpf et al. (2003). In Stumpf et al. (2004), multiple-radar data are combined into a rapidly updated 3D grid to derive several hail diagnosis parameters. By integrating all the information collected by multiple radars, it is possible to improve

the representation of the three-dimensional reflectivity field in the atmosphere, especially in single-radar cones-of-silence and at far range from one radar. This approach can also deal with storm tilt caused by fast-moving or highly-sheared storms. The processing of multiple-radar 3D data is not a trivial task and several approaches can be followed. In Zhang et al. (2005), various interpolation schemes are evaluated to convert multiple-radar reflectivity data onto a 3D multi-radar mosaic. It is found that simple and computationally efficient schemes allow the construction of a high-spatial- and high-temporal-resolution mosaic appropriate for operational applications.

Acknowledgements

References

Amburn, S. A. & Wolf, P. L. (1997) VIL density as a hail indicator. *Wea. Forecasting* **12**: 473–478.

Auer, A. H. Jr (1972) Distribution of graupel and hail with size. *Mon. Wea. Rev.* **100**: 325–328.

Auer, A. H. Jr (1994) Hail recognition through the combined use of radar reflectivity and cloud-top temperatures. *Mon. Wea. Rev.* **122**: 2218–2221.

Bech, J., Codina, B., Lorente, J. & Bebbington, D. (2003) The sensitivity of single polarization weather radar beam blockage correction to variability in the vertical refractivity gradient. *J. Atmos. Oceanic. Technol.* **20**: 845–855.

Collier, C. G. (1996) *Applications of Weather Radar Systems*. Chichester: Wiley, 390 pp.

Delobbe, L. & Holleman, I. (2003) Radar-based hail detection: Impact of height assignment errors on the measured vertical profiles of reflectivity. In *Preprints 31st Conference on Radar Meteorology*, Seattle, WA, Am. Meteorol. Soc. 475–478.

Delobbe, L. & Holleman, I. (2004) Quality of echotop products and derived probability of hail as a function of range. In *Proceedings of European Conference on Radar in Meteorology and Hydrology (ERAD)*, Gotland, Sweden: Copernicus GmbH, 87–90.

Delobbe, L., Holleman, I., Dehenauw, D. & Neméghaire, J. (2005) Verification of radar-based hail detection product. In *Preprints W.W.R.P. Symposium on Nowcasting and Very Short Range Forecasting (WSN05)*, Toulouse, France, P8.07.

Doviak, R. J. & Zrnic, D. S. (1993) *Doppler Radar and Weather Observations*, 2nd edn, San Diego: Academic Press, 562 pp.

Fraile, R., Castro, A., Sánchez, J. L., Marcos, J. L. & López, L. (2001) Noteworthy C-band radar parameters of storms on hail days in northwestern Spain. *Atmos. Res.* **59/60**: 41–61.

Gourley, J. J., Kaney, B. & Maddox, R.A. (2003) Evaluating the calibration of radars: a software approach. In *Preprints 31st Conference on Radar Meteorology*, Seattle, WA, Am. Meteorol. Soc., 459–462.

Greene, D. R. & Clark, R. A. (1972) Vertically integrated liquid water – a new analysis tool. *Mon. Wea. Rev.* **100**: 548–552.

Hardaker, P. J. & Auer, A. H. (1994) The separation of rain and hail using single polarization radar echoes and IR cloud-top temperatures. *Meteorol. Appl.* **1**: 201–204.

Holleman, I. (2001) Hail detection using single-polarization radar. Scientific report WR-2001-01, Royal Netherlands Meteorological Institute (KNMI), De Bilt, The Netherlands, 74 pp.

Holleman, I., Wessels, H. R. A, Onvlee, J. R. A. & Barlag, S. J. M. (2000) Development of a hail-detection-product. *Phys. Chem. Earth B* **25**: 1293–1297.

Howard, K. W., Gourley, J. J. & Maddox, R. A. (1997) Uncertainties in WSR-88D measurements and their impacts on monitoring life cycles. *Wea. Forecasting* **12**: 166–174.

Huuskonen, A. J. (2001) A method for monitoring the calibration and pointing accuracy of a radar network. In *Preprints 30th Conference on Radar Meteorology*, Munich, Germany, Am. Meteorol. Soc., 29–31.

Joe, P., Burgess, D., Potts, R., Keenan, T., Stumpf, G. & Treloar, A. (2004) The S2K severe weather detection algorithms and their performance. *Wea. Forecasting* **19**: 43–63.

Johnson, J. T., MacKeen, P. L., Witt, A., Mitchell, E. D., Stumpf, G. J., Eilts, M. D. & Thomas, K. W. (1998) The Storm Cell Identification and Tracking (SCIT) algorithm: an enhanced WSR-88D algorithm. *Wea. Forecasting* **13**: 263–276.

Kessinger, C. J., Brandes, E. A. & Smith, J. W. (1995) A comparison of the NEXRAD and NSSL hail detection algorithms. In *Preprints 27th Conference on Radar Meteorology*, Vail, CO, Am. Meteorol. Soc., 603–605.

Lemon, L. R. (1998) The radar 'three body scatter pike': an operational large-hail signature. *Wea. Forecasting* **13**: 327–340.

Lenning, E., Fuelberg, H. E. & Watson, A. I. (1998) An evaluation of WSR-88D severe hail algorithms along the northeastern Gulf Coast. *Wea. Forecasting* **13**: 1029–1044.

Lynn, R. J. & Lakshmanan, V. (2002) Virtual radar volumes: creation, algorithm access, and visualization. In *Preprints 21st Conf. on Severe Local Storm*, San Antonio, TX, Am. Meteorol. Soc., pp. 229–232.

Maddox, R. A., Zaras, D. S., MacKeen, P. L., Gourley, J. J., Rabin, R. & Howard, K. W. (1999) Echo height measurements with the WRS-88D: use of data from one versus two radars. *Wea. Forecasting* **14**: 455–460.

Marzban, C. & Witt, A. (2001) A Bayesian neural network for severe-hail size prediction. *Wea. Forecasting* **16**: 600–610.

Mason, B. J. (1971) *The Physics of Clouds*. Oxford: Clarendon Press, 670 pp.

Nanni, S., Mezzasalma, P. & Alberoni, P. P. (2000) Detection of hail by means of polarimetric radar data and hailpads: results from four storms. *Meteorol. Appl.* **7**: 121–128.

Scarchilli, G., Gorgucci, E., Chandrasekar, V. & Seliga, T. A. (1993) Rainfall estimation using polarimetric techniques at C-band frequencies. *J. Appl. Meteorol.* **32**: 1150–1159.

Stumpf, G. J., Smith, T. M. & Thomas, C. (2003) The National Severe Storms Laboratory's contribution to severe weather warning improvement: multiple-sensor severe weather applications. *Atmos. Res.* **67/68**: 657–669.

Stumpf, G. J., Smith, T. M. & Hocker, J. (2004) New hail diagnostic parameters derived by integrating multiple radars and multiple sensors. In *Preprints 22nd Conf. on Severe Local Storm*, Hyannis, MA, Am. Meteorol. Soc., P7.8.

Laurent Delobbe & Iwan Holleman

Tabary, P. (2003) Efforts to improve the monitoring of the French radar network. In *Preprints 31st Conference on Radar Meteorology*, Seattle, WA, Am. Meteorol. Soc., 482–485.

Treloar, A. (1998) Vertically integrated radar reflectivity as an indicator of hail size in the greater Sydney region of Australia. In *Preprints 19th Conference on Severe Local Storms*, Minneapolis, MN, Am. Meteorol. Soc., 48–51.

Waldvogel, A., Federer, B. & Grimm, P. (1979) Criteria for the detection of hail cells. *J. Appl. Meteorol.* **18**: 1521–1525.

Witt, A., Eilts, M. D., Stumpf, G. J., Johnson, J. T., Mitchell, E. D. & Thomas, K. W (1998) An enhanced hail detection algorithm for the WSR-88D. *Wea. Forecasting* **13**: 286–303.

Zhang, J., Howard, K. & Gourley, J. J. (2005) Constructing three-dimensional multiple-radar reflectivity mosaics: examples of convective storms and stratiform rain echoes. *J. Atmos. Oceanic. Technol.* **22**: 30–42.